factor replaced by a constant (constant radial matrix element approximation).

It is clear that a distorted-wave treatment of the data is required using realistic bound-state wave functions. The Q-value effect of the cross sections must also be considered in a correct treatment of the data. As the neutron number in the sequence of Sn isotopes increases, the neutrons become less bound and the Q values less negative. If the (p,t) reaction occurs at the nuclear surface, this effect would tend to increase the pickup cross section in the heavier isotopes. That is, if included in the predicted "pairing spectroscopic factors" shown in Fig. 6, the effect would tend to make the discrepancy even larger. It is not clear, however, just how the binding energies should be treated in the DWBA analysis.

The disagreement between the experiment and theory may, however, be due to the assumed configuration of neutrons in the Sn isotopes. The U_j's and V_j's that have been used involve only the neutrons outside the closed-shell core of 50 protons and neutrons. However, for the lighter Sn isotopes it may be necessary to include the effect of some excitation of the closed neutron shells in the ground states. Presumably this effect will be less pronounced for the heavier isotopes. This effect would increase the cross sections predicted for the lighter Sn isotopes and account for some of the discrepancy between the theory and the data. A similar discrepancy with pairing theory has been seen for the Ni isotopes.[1]

The Cd $L=0$ integrated cross sections shown in Fig. 6 are smaller than for the corresponding Sn isotopes, as might be expected. The effect of opening the closed proton shell would tend to introduce components into the wave functions with neutron and proton spins not separately zero, thus decreasing the number of $J=0$ coupled neutron pairs and hence the $L=0$ cross sections. A similar effect has already been observed in comparing the Fe isotopes to the Ni isotopes.[1] The apparent agreement of the Cd data with the theoretical curve for Sn is probably coincidental.

Note added in proof. In order to check the relative-target-thickness measurements, the elastic scattering yield of 40-MeV protons from Cd in the four CdO targets has recently been measured over the peak in the angular distribution near 50°. The relative spectroscopic factors shown in Fig. 6 were not changed by more than the 15% errors on the data.

PHYSICAL REVIEW VOLUME 139, NUMBER 4B 23 AUGUST 1965

Measurement and Statistical Theory Analysis of $Fe^{56}(He^3,p)$ and $Cu^{63}(He^3,p)$ Energy and Angular Distributions–Nuclear Shell Effects*

JEAN-PIERRE HAZAN† AND GEORGE MERKEL‡
Department of Chemistry, University of Rochester, Rochester, New York
(Received 13 April 1965)

Thin Fe^{56} and Cu^{63} targets (approximately 1.5 mg/cm²) were bombarded with 10-MeV He^3 particles. The proton energy and angular distributions produced by the $Fe^{56}(He^3,p)$ and $Cu^{63}(He^3,p)$ reactions were measured by the $E-\Delta E$ particle identification technique. In the statistical theory interpretation of the experimental cross sections both the shape and magnitude of the angular and energy distributions were calculated. Contributions from the (He^3,np) and $(He^3,2p)$ reactions were also calculated. Large sections of the measured proton energy and angular distributions (about 90% of the total cross sections) are consistent with the predictions of the statistical theory of compound-nucleus reactions. A conventional statistical theory calculation of the $Cu^{63}(He^3,p)$ cross sections is generally consistent with the experimental cross sections; however, a similar conventional calculation of the $Fe^{56}(He^3,p)$ cross sections yields values 50% smaller than the experimental results. Rosenzweig has derived an expression for nuclear level densities which indicates that level densities of nuclei in the immediate vicinity of the doubly closed shell Ni^{56} nucleus can be influenced by nuclear shell structure at excitation energies as high as 15 MeV. A second statistical theory calculation of the magnitude and shape of the $Fe^{56}(He^3,p)$ cross sections, based on the Rosenzweig level density expression, yields calculated cross sections generally consistent with the measured $Fe^{56}(He^3,p)$ cross sections.

I. INTRODUCTION

IN this paper we describe the measurement of proton energy and angular distributions produced by bombarding Fe^{56} and Cu^{63} targets with 10-MeV He^3 ions, and present a statistical theory analysis of those portions of the cross-section measurements which are consistent with statistical theory. We were interested in determining the magnitude of the compound-nucleus contribution to these reactions, in the possibility of using (He^3,p) compound-nucleus reactions to obtain information about nuclear level densities, and in the

* Work supported by the U. S. Atomic Energy Commission.
† Part of this work was done in conjunction with another study as partial fulfillment of the Ph.D. requirement at the University of Rochester. Now on active duty in Armée de la République Française. Permanent address: 146 Rue de Tocqueville, Paris 17e, France.

‡ Present address: General Atomic Division of General Dynamics, John Jay Hopkins Laboratory for Pure and Applied Science, San Diego, California.

influence of nuclear shell structure on nuclear level densities. A number of authors, e.g., Margenau,[1] Bloch,[2] Newton,[3] Ross,[4] and Rosenzweig[5,6] have indicated that nuclear shell structure can influence nuclear level densities at relatively high excitation energies (up to 10 or 20 MeV). Excitation function experiments which are generally consistent with the predictions of the above authors have been reported.[7–15]

The $Fe^{56}(He^3,p)Co^{58}$ reaction is of interest because the formation of Co^{58} is in direct competition with the formation of the closed shell Ni^{58} nucleus by the $Fe^{56}(He^3,n)Ni^{58}$ reaction. In the statistical theory analysis of the proton spectra we first employ a nuclear level density expression in which nuclear shell structure is neglected; we then take nuclear shell structure into consideration by employing a nuclear level density expression derived by Rosenzweig.[5,6] The absolute experimental cross sections and also the shape of the energy and angular distributions are compared with the statistical theory predictions.

II. EXPERIMENTAL DETERMINATION OF $Fe^{56}(He^3,p)$ CROSS SECTIONS

1. Equipment

The experiment was performed at the University of Rochester 27-in. variable energy cyclotron, which is capable of accelerating He^3 from 8 to 11 MeV. The external beam was brought through steering magnets and two sets of focusing lenses to a target chamber. The collimation system at the target chamber end consisted of two slits and one antiscattering slit. The beam spot on the target was approximately $\frac{1}{16}$ in.$\times\frac{1}{4}$ in.

The incident-beam current was determined with a surface barrier Si counter placed to monitor the He^3 elastic scattering at 45°, where Rutherford scattering constitutes the near totality of the counts observed. The counter pulses were fed into a scaler with a discriminator set to eliminate electronic noise.

The target was a self-supported Fe^{56} foil of 99.7% purity purchased from the Oak Ridge National Laboratory. The target thickness was determined by weighing, and also by measuring the energy loss of Pu α particles in the foil. It was found to be 1.5 mg/cm^2. Several measurements performed by the latter method at different positions indicated a uniformity of $\pm 3\%$.

An $E-\Delta E$ counter telescope system was used. A collimator 0.638 cm in diameter was placed in front of the counters at 9.5 cm from the target holder. The solid angle subtended was 3.3 10^{-3} sr. The E counter was a 3-mm-thick Li-drifted surface barrier detector capable of stopping 23-MeV protons. The ΔE counter was a 2.3-mil totally depleted Si detector, thick enough to provide good resolution in the particle identification system and to resolve deuterons from protons. The particle identification procedure made use of the standard $E\times\Delta E$ pulse multiplication methods. The multiplier used was designed by Chase and modified by Swenson.[16] A block diagram of the multiplier and associated electronics is shown in Fig. 1.

The effectiveness of the experimental particle identification system in discriminating between protons and deuterons is illustrated in Fig. 2, which shows simultaneously measured deuteron and proton spectra. As can be seen there is no correlation between the proton spectrum and the peaks in the deuteron spectrum. The range of the elastically scattered He^3 particles was not great enough to penetrate through the ΔE counter into the E counter.

2. Experimental Procedures

The value of the incoming He^3 energy, determined by magnetic analysis, was 10.25 MeV (± 0.05 MeV). When the average target thickness was taken into account, the incident energy at the center of the target was found to be about 10.0 MeV (the value of dE/dx for He^3 in Fe at 10.0 MeV is 0.25 MeV/mg).

Spectra at nine different angles were observed: 150°, 135°, 120°, 110°, 90°, 75°, 60°, 45°, and 30°. These spectra were collected by two different procedures: (1) From

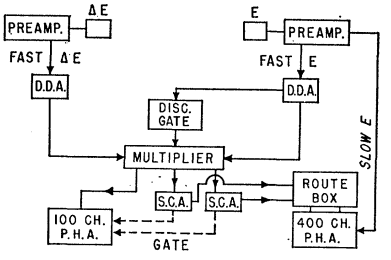

FIG. 1. Block diagram of electronics, showing arrangement of preamplifiers, double delay line amplifiers, discriminator-gates, multiplier, single-channel analyzers, and pulse-height analyzers. The 100-channel pulse-height analyzer recorded the multiplied pulses. The 400-channel pulse-height analyzer recorded the proton and deuteron spectra.

[1] H. Margenau, Phys. Rev. **59**, 627 (1941).
[2] C. Bloch, Phys. Rev. **93**, 1094 (1954).
[3] T. D. Newton, Can. J. Phys. **34**, 804 (1956).
[4] A. A. Ross, Phys. Rev. **108**, 720 (1957).
[5] N. Rosenzweig, Phys. Rev. **108**, 817 (1957).
[6] N. Rosenzweig, L. M. Bollinger, L. L. Lee, and J. P. Schiffer, in *Proceedings of the Second United Nations International Conference on the Peaceful Uses of Atomic Energy, Geneva, 1958* (United Nations, Geneva, 1958).
[7] G. Merkel, University of California Radiation Laboratory Report No. UCRL-9898, 1961 (unpublished).
[8] M. Blann and G. Merkel, Nucl. Phys. **52**, 673 (1964).
[9] M. Blann, F. M. Lanzafame, and R. A. Piscitelli, Phys. Rev. **133**, B700 (1964).
[10] M. Blann, Phys. Rev. **133**, B707 (1964).
[11] M. Blann and A. Ewart, Phys. Rev. **134**, B783 (1964).
[12] Jean-Pierre Hazan, Ph.D. thesis, University of Rochester, 1964 (unpublished).
[13] A. Ewart, Ph.D. thesis, University of Rochester, 1964 (unpublished).
[14] M. Blann and G. Merkel, Phys. Rev. **137**, B367 (1965).
[15] J.-P. Hazan and M. Blann, Phys. Rev. **137**, B1202 (1965); this paper is based on Ref. 12.
[16] W. Swenson, Ph. D. thesis, MIT, 1963 (unpublished).

150 to 60° inclusive, no absorber was used. The threshold due to the ΔE counter thickness was 2.7 MeV. Actually with the E discriminator gate, the detection threshold was raised to about 3.2 MeV in the proton laboratory energy E_{lab}. (2) At 45° and 30°, an Al absorber was placed in front of the detector system to prevent pulses from the elastically scattered He^3 from "piling up" in the ΔE counter. The absorber was 19.7 mg/cm². Absorber homogeneity was checked by cutting the original piece into smaller pieces. It was found to be homogeneous within 2–3%. The thickness of the absorber and the ΔE counter results in a 4-MeV detection threshold for protons. The discriminator raised the threshold to about 4.6-MeV proton lab energy. To check reproducibility, a few of the backward angle measurements were repeated with the absorber.

The proton-energy spectra from 3.5 to 14 MeV were calibrated with proton peaks from the $C^{12}(He^3,p)N^{14}$ reaction and the so-called "knock-on protons" from the

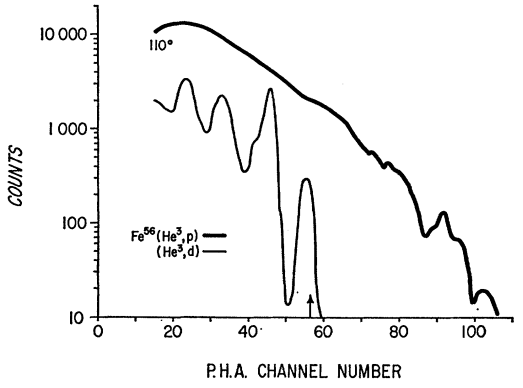

FIG. 2. Proton and deuteron spectra—simultaneously obtained by bombarding Fe^{56} with 10-MeV He^3 particles. The arrow corresponds to the ground state of Mn^{55}.

$H(He^3,p)He^3$ reaction. These spectra were obtained with a thin polyethylene target. As a check for electronic drift a polyethylene proton spectrum was measured immediately after each Fe^{56} proton spectrum measurement. Independent forward angle polyethylene spectra were also measured, as well as "knock-on proton" spectra from 40°–50°. The angles could be read to a precision of 0.1°.

A great number of overlapping calibration points which agreed closely with each other (within 100 keV) were thus obtained. An additional check on the consistency of the calibration was made by plotting the energy actually observed in the analyzer versus the channel number. This energy was determined from the calibration points by taking into account the absorption effect of the target and the ΔE counter. This plot, together with the calibration curve, is shown in Fig. 3, and is a straight line going through channel 0 at 0 MeV as expected.

A similar check was made for the energy calibration

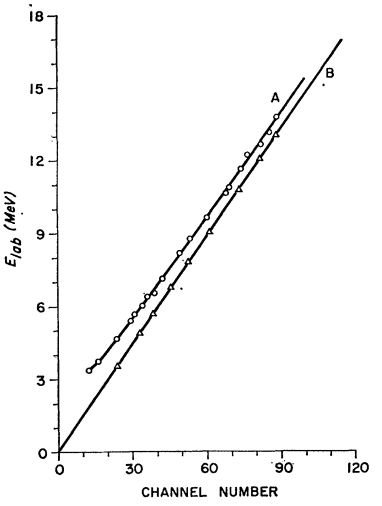

FIG. 3. Calibration curves based on kinematics of known carbon and oxygen levels. The points on curve A are experimentally determined; the points on curve B are calculated from curve A by subtracting the proton energy lost in the ΔE counter.

curve obtained with the aluminum absorber in front of the counter. Deviation of calibration points from the curve was within 50–75 keV (about half a channel), which is within the beam energy uncertainty and beam spread. At the very low energy end of the curve (below 4.5 MeV for the nonabsorption curve) the scatter of the calibration points is somewhat larger (but within ±100 keV).

The determination of the effect of C, O, and H target foil contamination was simplified because the $C(He^3,p)$, $O(He^3,p)$, and "knock-on proton" spectra consist of well-resolved peaks. These spectra were taken with polyethylene and Mylar targets. Figure 4 shows that there was usually very little correlation between the Mylar spectra and the Fe spectra, especially in the continuum region. In the most severe cases, only 2 or 3 "humps" in the continuum correlated with the C spectrum. These "humps" covered 6 or 7 channels and did not constitute more than 5–10% of the counts at

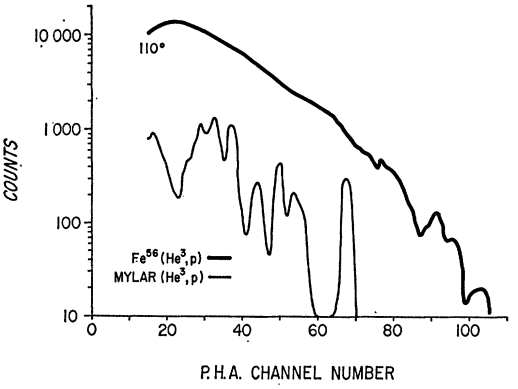

FIG. 4. Proton spectra obtained by bombarding Mylar and Fe^{56} with 10-MeV He^3 particles.

those points. We have not attempted to subtract them. The exception is the 30° proton spectrum, where high-energy peaks correlated with carbon peaks and normalization was possible. The correction in the continuum was very small (±1–2%) except for the 2–3 "humps" just mentioned. At 30° a very prominent "knock-on proton" peak appeared between channels 18 and 26, making the cross-section determinations uncertain at the equivalent energies. These channels, corresponding to energies below 6 MeV $E_{c.m.}$, are not included in the final presentation of experimental cross sections. No targets containing nitrogen were used to check for nitrogen contamination; however, several proton groups leading to the O^{16} low-lying levels would have had their energies above the maximum proton energy of the $Fe^{56}(He^3,p)$ reaction. Such peaks were not observed.

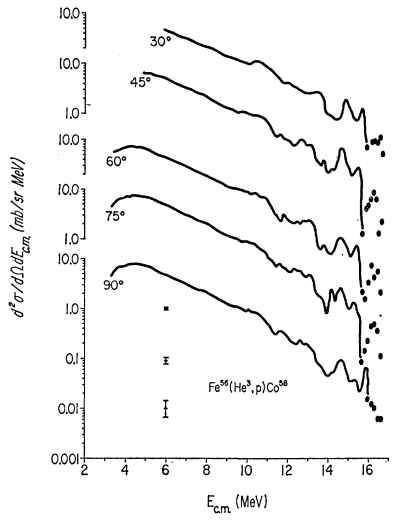

FIG. 5. Fe(He³,p) energy spectra obtained at various forward angles.

3. Data Processing

The following corrections were applied to the original data: (1) The pulse-height-analyzer channel number was transformed to proton laboratory energy by using the calibration curves discussed in Sec. II 2. (2) The proton energy loss in the ΔE counter and the Al absorber foil varied as a function of laboratory energy, E_{lab}; therefore, the pulse-height-analyzer channel width was corrected to correspond to the laboratory energy channel width by multiplying the pulse-height counts in channel C by $(\Delta C/\Delta E_{lab})$ at the corresponding E_{lab}.[17] (3) The absolute laboratory cross sections were determined with the monitor counts and the Rutherford cross section. (4) The center-of-mass cross section was determined from the laboratory cross section with the relation

$$d^2\sigma/d\Omega dE_{c.m.} = (E_{c.m.}/E_{lab})^{1/2}(d^2/d\Omega dE_{lab}).$$

The experimentally determined $Fe^{56}(He^3,p)$ energy and angular distributions, corrected to the center-of-mass coordinate system, are shown in Figs. 5, 6, and 7. For reasons of clarity, the proton energy distributions shown in Figs. 5 and 6 have each been displaced by a decade. For comparison, the 135° and 75° proton energy distributions have been superimposed in Fig. 8.

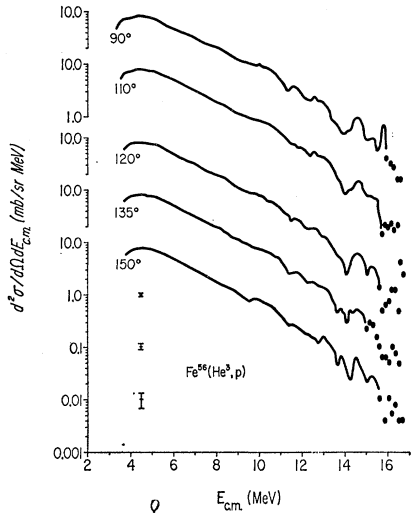

FIG. 6. Fe(He³,p) energy spectra obtained at various backward angles.

III. EXPERIMENTAL DETERMINATION OF $Cu^{63}(He^3,p)$ CROSS SECTIONS

The equipment, experimental procedures, and data treatment were essentially the same as in the $Fe^{56}(He^3,p)$ cross section measurements except that, because of cyclotron time limitations, data were obtained only for angles larger than 90°. The final center-of-mass results are shown in Figs. 9 and 10.

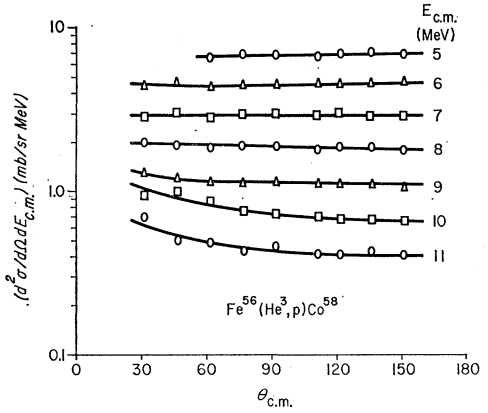

FIG. 7. Fe(He³,p) angular distributions.

[17] J. Benveniste, R. Booth, and A. Mitchell, University of California Radiation Laboratory Report No. UCRL-7427, 1963 (unpublished).

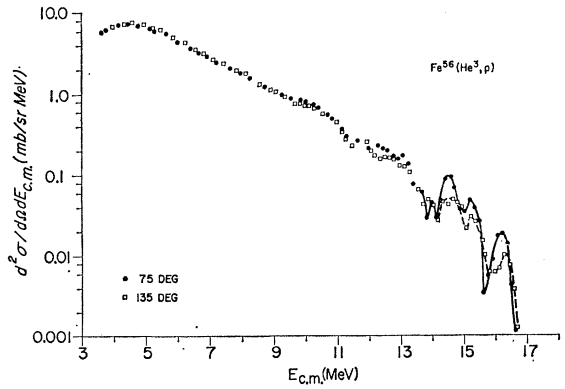

FIG. 8. Superposition of $Fe^{56}(He^3,p)$ spectra obtained at 75° and 135°.

IV. NUCLEAR LEVEL DENSITY EXPRESSIONS

If a nuclear reaction proceeds by the compound-nucleus reaction mechanism, the magnitude of angular and energy distributions can be calculated if the distributions of nuclear energy and spin states in the various species of residual nuclei are known.

Nuclear level densities have been discussed by many authors. The nuclear level density $\rho(U,J)$ for a nucleus with excitation energy U and spin J is usually expressed as[4,18,19]

$$\rho(U,J)=C_1(2J+1)U^{-2}\exp[2(aU)^{1/2}] \times\exp(-J^2/\sigma^2), \quad (1)$$

where, for a specific nucleus, C_1 remains a constant, a is the nuclear level density parameter, and σ^2 is the spin cutoff parameter. The parameter a is related to the average nucleon level spacing δ at the Fermi level[18]:

$$a=(\pi^2/6)(1/\delta). \quad (2)$$

If nuclear shell effects are neglected, the nuclear level density parameter is usually assumed to be related to the nuclear mass number A by an expression of the form $a=(\text{const})A$, e.g., $a=A/8$.[18] Newton,[3] and also Lang,[20] have made semiempirical estimates of the influence of nuclear shell structure on a or δ. According to Lang

$$a=0.0748(\bar{j}_n+\bar{j}_p+1), \quad (3)$$

where $\bar{j}_n$ and $\bar{j}_p$ are the means of j values for neutrons and protons, respectively, in the vicinity of the Fermi level of the nucleus being considered. Newton has listed the values of $\bar{j}_n$ and $\bar{j}_p$ for all nuclei.[3]

The density of nuclear levels at excitation energy U can be expressed as[18–22]

$$\rho(U)=C_2U^{-5/4}\exp[2(aU)^{1/2}], \quad (4)$$

where, for a specific nucleus C_2 remains constant; however, an expression of the form[19,23]

$$\rho(U)=C_3U^{-2}\exp[2(aU)^{1/2}] \quad (5)$$

is frequently used in statistical theory calculations. The justification for Eq. (5) is that evaporated particles tend to decay into a narrow region of spins.[19]

Equations (1), (2), and (3) are all based on the assumption of a continuous distribution of nucleon levels in the vicinity of the Fermi level.[2] A number of authors have examined the influence of discrete nucleon level structure on nucleon level density.[1–6] In the region adjacent to closed shells, nuclear structure can cause large deviations. For example, if a shell is partly filled, the nucleons in the incomplete shell can be arranged in many ways with no expenditure of energy, and the nuclear level density would be increased. On the other hand, if the shell is completely filled, energy must be expended to lift nucleons up to the next shell, and the nuclear level density would be decreased.[2,7,8]

Rosenzweig[5,6] employed a simplified nuclear model to obtain a closed-form expression that considered discrete nucleon level spacing. In Rosenzweig's model the nucleus consists of two kinds of Fermi particles, each occupying uniformly spaced energy levels. The degeneracy of each level is the same, although the degeneracies for different particles, i.e., neutrons and protons, can be different. For the neutron system, let n be the number of neutrons or neutron holes in the Fermi level, g the degeneracy of each nuetron level, and γ the spacing between adjacent levels. For the proton system, let p be the number of protons or proton holes in the Fermi level, e the degeneracy of each level,

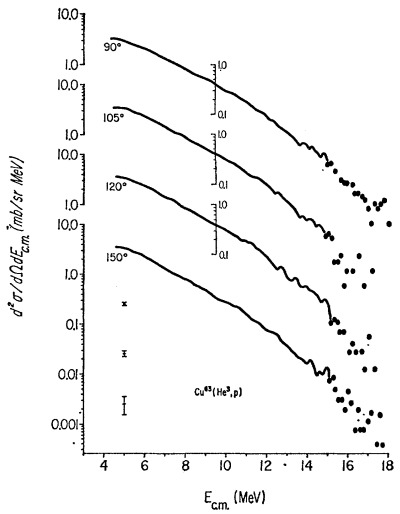

FIG. 9. $Cu(He^3,p)$ energy spectra.

[18] T. Ericson, Advan. Phys. **9**, 427 (1960).
[19] D. Bodansky, Ann. Rev. Nucl. Sci. **12**, 79 (1962).
[20] D. W. Lang, Nucl. Phys. **26**, 434 (1961).
[21] C. van Lier and G. E. Uhlenbeck, Physica **4**, 531 (1937).
[22] H. Bethe, Rev. Mod. Phys. **9**, 69 (1937).
[23] T. Ericson, *Proceedings of the International Conference on Nuclear Structure, Kingston, Canada, 1960,* edited by D. A. Bromley and E. Vogt (University of Toronto Press, Toronto, 1960), p. 697.

and ϵ the spacing between adjacent levels. If $\Delta^{-1}=g/\gamma+e/\epsilon$, the nuclear level density expression derived by Rosenzweig is[5,6]

$$\rho(Q)=C_4Q^{-5/4}\exp\{\pi[\tfrac{2}{3}(Q/\Delta)]^{1/2}\}, \quad (6)$$

where

$$Q=U+\tfrac{1}{12}(g\gamma)-\frac{\gamma}{2g}(n-\tfrac{1}{2}g)^2+\tfrac{1}{12}(e\epsilon)-\frac{\epsilon}{2e}(p-\tfrac{1}{2}e)^2, \quad (6')$$

U is the excitation energy of the nucleus, and C_4 can be expressed in terms of g/γ and e/ϵ. The essential difference between Eqs. (1) and (4) is a shift in excitation energy. An estimate of the value of γ and ϵ for nuclei in the immediate vicinity of Ni^{56} can be obtained with Nilsson's[24] nucleon level distributions from the difference between the $2p_{3/2}$ and $1f_{7/2}$ subshells in a spherical nucleus with mass 56; the assumption that $\hbar\omega_0=41A^{-1/3}$ yields $\gamma=\epsilon=3$ MeV. The degeneracies of the $2p_{3/2}$ and $1f_{7/2}$ subshells can be averaged to obtain $g=e=6$. Then

$$Q=U+\Delta E=U+3+\tfrac{1}{4}(n-3)^2+\tfrac{1}{4}(p-3)^2, \quad (7)$$

where n and p are the number of neutrons and protons, respectively, that must be added or subtracted to obtain a nucleus with 28 neutrons and protons.

Residual interactions between nucleons are not considered in the derivation of the foregoing equations. In the treatment of residual interactions it is common, if not completely rigorous, to introduce a pairing energy that must be supplied to the nucleus before it is treated as a noninteracting Fermi gas.[2,25,26] The pairing energy is simply subtracted from the excitation energy before substitution into the independent particle level density equations; i.e., $U-\Delta U$ is substituted for U in Eqs. (1) or (7). In the nuclei considered in this paper we use $\Delta U=0$, 1.4, or 2.8 for odd-odd, even-odd, or even-even nuclei, respectively.[8,27,28]

V. ANGULAR DISTRIBUTIONS

As shown in Figs. 7 and 10 the angular distributions of the protons in the $Fe^{56}(He^3,p)$ and $Cu^{63}(He^3,p)$ reactions are essentially isotropic for angles greater than 90°. The divergence from isotropy at high proton emission energies and forward angles, Fig. 7, may be explained in terms of the low probability of high-energy compound-nucleus protons as compared to the probability of nonrandom direct-reaction protons.

Ericson and Strutinski have calculated the angular distribution of emitted particles predicted by the statistical theory. To a first approximation, the angular distribution is given by[18,29]

$$W(\theta)\approx 1+(\langle I^2\rangle_{\rm av}\langle l^2\rangle_{\rm av}/12\sigma^2)\cos\theta, \quad (8)$$

where σ^2 is the spin cutoff parameter of the residual nucleus; and where the quantities $\langle I^2\rangle_{\rm av}$ and $\langle l^2\rangle_{\rm av}$ are the mean-square values of the angular momentum quantum numbers of the bombarding and emitted particles, respectively.

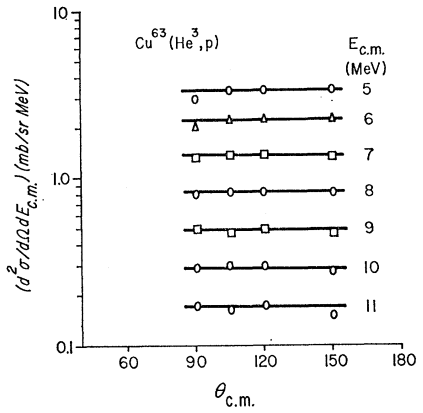

FIG. 10. $Cu(He^3,p)$ angular distributions.

We calculate $\langle I^2\rangle_{\rm av}$ and $\langle l^2\rangle_{\rm av}$ with optical model transmission coefficients for 10-MeV He^3 and 8-MeV protons corresponding to the $Fe^{56}(He^3,p)$ reaction and obtain $\langle I^2\rangle_{\rm av}=10$ and $\langle l^2\rangle_{\rm av}=4$.[8,10,30–32] An experimental determination of the spin cutoff parameter of Fe^{56} at 8-MeV excitation from $Fe(\alpha,\alpha')Fe^*$ scattering yields $\sigma^2=11.1$.[33] We can, therefore, estimate that the value of $(\langle I^2\rangle_{\rm av}\langle l^2\rangle_{\rm av}/12\sigma^2)$ corresponding to the $Fe^{56}(He^3,p)$ reaction is approximately 0.02–0.03. The value of $(\langle I^2\rangle_{\rm av}\langle l^2\rangle_{\rm av}/12\sigma^2)$ corresponding to the $Cu^{63}(He^3,p)$ reaction is less than 0.02. Therefore, we expect the experimental (He^3,p) angular distributions for Fe^{56} and Cu^{63} to be essentially isotropic. The experimental angular distributions shown in Figs. 7 and 10 are indeed isotropic.

VI. LEVEL DENSITY PARAMETER a AND PROTON SPECTRUM SHAPE

1. Determination of a with Weisskopf-Ewing Statistical Theory

In the case of isotropic angular distributions where both $I_{\rm av}$ and $l_{\rm av}$ are relatively small, the coupling of **I** to **l** is generally weak and the neglect of angular-

[24] S. C. Nilsson, Kgl. Danske Videnskab. Selskab, Mat. Fys. Medd. **29**, (1955).
[25] H. Hurwitz and H. Bethe, Phys. Rev. **81**, 898 (1951).
[26] T. Ericson, Nucl. Phys. **6**, 62 (1958).
[27] F. Everling, L. A. König, and J. H. E. Mattauch, Nucl. Phys. **18**, 529 (1960).
[28] P. E. Nemirovsky and Yu. V. Adamchuk, Nucl. Phys. **39**, 551 (1962).
[29] T. Ericson and V. Strutinski, Nucl. Phys. **8**, 284 (1958); **9**, 689 (1959).
[30] F. E. Bjorklund and S. Fernbach, in *Proceedings of the Second United Nations International Conference on the Peaceful Uses of Atomic Energy, Geneva, 1958* (United Nations, Geneva, 1958), Vol. 14, p. 24.
[31] G. S. Mani, M. A. Melkanoff, and I. Iori, Centre d'Etudes Nucléaires de Saclay, Report No. 2379, 1963 (unpublished).
[32] The He^3 optical-model parameters are discussed in Sec. VII 1.
[33] J. Benveniste, G. Merkel, and A. Mitchell (unpublished).

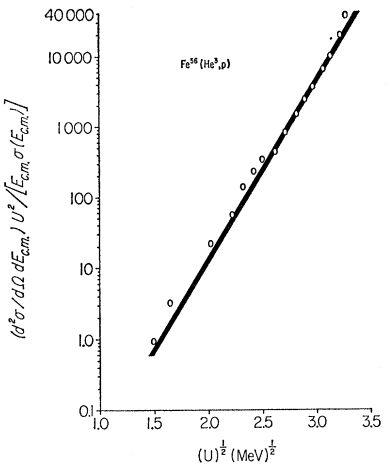

FIG. 11. Semilogarithmic plot for the determination of the nuclear level density parameter a from the $Fe^{56}(He^3,p)Co^{58}$ reaction.

momentum restrictions becomes valid.[18] Under these conditions the conventional statistical theory as first presented by Weisskopf and Ewing[34–36] is, with slight modifications, a good approximation to the more accurate development of Ericson and Strutinski.[29]

If we consider only protons that are emitted from the primary compound nucleus, and if we introduce the nucleon pairing energy ΔU, the differential cross section per unit channel energy is

$$\frac{d^2\sigma}{d\Omega dE_{c.m.}}=\frac{(\text{const})E_{c.m.}\sigma(E_{c.m.})}{(U-\Delta U)^2}\times\exp\{2[a(U-\Delta U)]^{1/2}\}, \quad (9)$$

where $\sigma(E_{c.m.})$ is the capture cross section of the emitted particle (in this case a proton) with channel energy $E_{c.m.}$, and U is the excitation energy of the residual nucleus. Thus according to Eq. (9) a semilogarithmic plot of the expression

$$\left(\frac{d^2\sigma}{d\Omega dE_{c.m.}}\right)\frac{(U-\Delta U)^2}{E_{c.m.}\sigma(E_{c.m.})} \quad (10)$$

as a function of $(U-\Delta U)^{1/2}$, where Eq. (10) is calculated with experimentally determined values of $d^2\sigma/d\Omega dE_{c.m.}$ should yield a straight line, the slope of which is the value of $2a^{1/2}$.

From the semilogarithmic plots for the $Fe^{56}(He^3,p)Co^{58}$ and $Cu^{63}(He^3,p)Zn^{65}$ reactions, shown in Figs. 11 and 12, we determine $a=8.7$ MeV^{-1} for the Co^{58} residual nucleus and $a=7.0$ MeV^{-1} for the Zn^{65} residual nucleus. The divergence from the straight line in the low proton emission energy region of the semilogarithmic plots is consistent with the presence of multiple particle emissions such as occur in (He^3,np) and $(He^3,2p)$ reactions. A comparison of Figs. 11 and 12 indicates that the $Fe^{56}(He^3,p)$ semilogarithmic plot has a greater divergence from the straight line at low excitation energies than the $Cu^{63}(He^3,p)$ plot. Divergence from the straight line in the region corresponding to high proton emission energies is consistent with the presence of direct interactions, but we can offer no explanation for the greater divergence in the case of the Fe^{56} reaction. The statistical theory cross sections for the emission of high-energy protons are very small, and as Ericson has indicated, the statistical theory is expected to give the lower limit to an experimental cross section.[18]

A better visualization of the agreement between the experimental results and the predictions of Eq. (9) can be obtained by using the values of the parameter a obtained with the semilogarithmic plots and arbitrarily normalizing the calculated proton energy spectra shapes to the experimental spectra. The arbitrarily normalized curves for the $Fe^{56}(He^3,p)$ and $Cu^{63}(He^3,p)$ reactions are shown in Figs. 13 and 14.

The values of a obtained for Co^{58} and Zn^{65} from the experimental $Fe^{56}(He^3,p)Co^{58}$ and $Cu^{63}(He^3,p)Zn^{65}$ cross sections are generally consistent with a cluster of values of the parameter a obtained by Lang[20,37] from the analysis of particle spectra data in this region of the chart of nuclides. The same form of level density was used for the analysis of the latter data as was used in this work. Glover and Purser[38] have determined a value of 7.8 MeV^{-1} for a from the $Ni^{58}(n,p)Co^{58}$ reaction. These authors, however, used a different set of values for the proton inverse cross sections. Bodansky[19] notes that with present methods of analysis, when a values

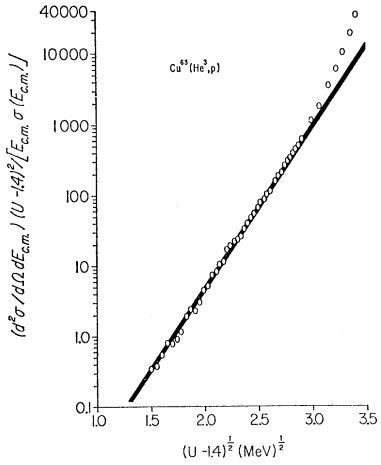

FIG. 12. Semilogarithmic plot for the determination of the nuclear level density parameter a from the $Cu^{63}(He^3,p)Zn^{65}$ reaction.

[34] V. F. Weisskopf, Phys. Rev. **52**, 295 (1937).
[35] V. F. Weisskopf and D. H. Ewing, Phys. Rev. **57**, 472 (1940).
[36] J. Blatt and V. Weisskopf, *Theoretical Nuclear Physics* (John Wiley & Sons, Inc., New York, 1952) p. 365.
[37] R. W. West, Ph.D. thesis, University of Washington, 1964 (unpublished).
[38] R. N. Glover and K. H. Purser, Nucl. Phys. **24**, 431 (1961).

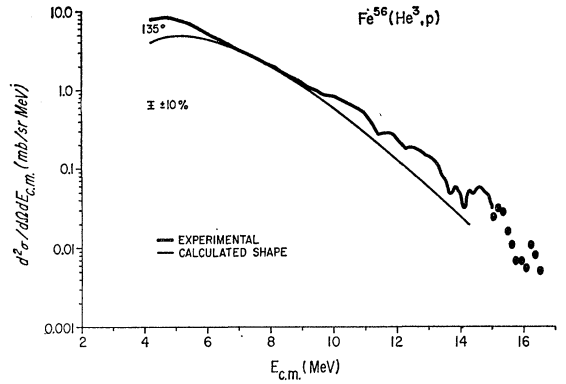

FIG. 13. Experimental $Fe^{56}(He^3,p)$ proton spectrum plus an arbitrarily normalized statistical theory $Fe^{56}(He^3,p)Co^{58}$ proton spectrum.

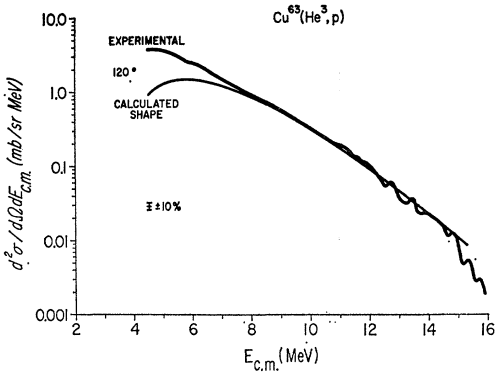

FIG. 14. Experimental $Cu^{63}(He^3,p)$ proton spectrum plus an arbitrarily normalized statistical theory $Cu^{63}(He^3,p)Zn^{65}$ proton spectrum.

are found to be consistent within 10–15%, the agreement is considered to be good.

2. The Nuclear Level Density Parameter a and the Ericson-Strutinski Statistical Theory

The parameter a can also be determined with the Ericson and Strutinski statistical theory, which is based on the more realistic assumption that the nuclear level density in residual nuclei with spin J is proportional to $(2J+1)\exp(J^2/2\sigma^2)$ rather than $(2J+1)$.[29] At the excitation energy encountered in these experiments, proton and neutron emission account for the largest part of compound-nucleus decay. The optical model yields an estimate of the largest significant angular momentum values of the compound nucleus and the emitted particles; e.g., for 10-MeV He^3 ions incident on Fe^{56}, $I=5$ accounts for only 3% of the total cross section due to all I, and for 6-MeV protons incident on Co^{58}, $l=4$ accounts for only 3% of the total cross section due to all l. If $I\leq 5$ and $l\leq 4$, a very accurate approximation to the Ericson and Strutinski differential cross section is given by

$$\frac{d^2\sigma}{d\Omega dE_\nu}=\frac{g_\nu\mu_\nu\lambda_\nu^2}{4\pi}E_\nu\frac{\exp\{2[a(U_\nu-\Delta U_\nu)]^{1/2}\}}{(U_\nu-\Delta U_\nu)^2}\int_0^\infty dI(2I+1)T_I\lambda_i^2$$
$$\times\left[\int_0^\infty dl(2l+1)T_l(E_\nu)\exp\left(-\frac{I^2+l^2}{2\sigma_\nu^2}\right)\left\{j_0\left(i\frac{Il}{\sigma_\nu^2}\right)-\frac{5}{4}j_2\left(i\frac{Il}{\sigma_\nu^2}\right)P_2(\cos\theta)+\cdots\right\}\right]\Big/$$
$$\left[\sum_\nu\lambda_\nu^2 g_\nu\mu_\nu\int_0^{E_{\nu,\max}}dE_\nu\int_0^\infty dl(2l+1)E_\nu T_l(E_\nu)\frac{\exp\{2[a(U_\nu-\Delta U_\nu)]^{1/2}\}}{(U_\nu-\Delta U_\nu)^2}\exp\left(-\frac{I^2+l^2}{\sigma_\nu^2}\right)j_0\left(i\frac{Il}{\sigma_\nu}\right)\right]. \quad (11)$$

The T_I are the transmission coefficients for the bombarding He^3 ion; the $T_l(E_\nu)$ are the transmission coefficients for the emitted particle ν, g_ν is the statistical weight factor due to spin of particle ν; μ_ν is the reduced mass and E_ν the channel energy of particle ν; U_ν is the excitation energy and σ_ν^2 the spin cutoff parameter of the residual nucleus produced by the emission of particle ν, and ΔU_ν the appropriate pairing energy correction as described in Sec. IV; we carry out the summation over neutrons, protons, and alpha particles. The energy $E_{\nu,\max}$ is the maximum energy of particle ν.[39,40] A determination of the nuclear level parameter a that is based on the experimental $Fe^{56}(He^3,p)$ cross sections and Eq. (11), in which we make the extreme assumption that $T_I=0$ for all values of I except $I=5$, yields a value of a that agrees to within 6% of the value of a determined with the simple Weisskopf-Ewing theory, Eq. (9). Parallel calculations with $I<5$ would yield differences of less than 6%.

VII. ABSOLUTE CROSS-SECTION CALCULATIONS

1. Conventional Calculation

An absolute cross-section calculation based on the Weisskopf-Ewing statistical theory that does not involve the consideration of cascade emission is rela-

[39] The appearance of the factor $(U_\nu-\Delta U_\nu)^{-2}$ in Eq. (14) supports the use of the factor $(U-\Delta U)^{-2}$ in Eq. (9).

[40] The calculation of the transmission coefficients $T_l(E_\nu)$ is described in Ref. 12. The calculation of T_I is described in Sec. VII 1.

tively simple. The differential cross section is

$$\frac{d^2\sigma}{d\Omega dE_\nu}=\frac{\sigma_c}{4\pi}[g_\nu\mu_\nu E_\nu\sigma_\nu(E_\nu)\rho(U_\nu-\Delta U_\nu)]/$$
$$\left[\sum_\nu g_\nu\mu_\nu\int_0^{E_{\nu,\max}}E_\nu\sigma_\nu(E_\nu)\rho(U_\nu-\Delta U_\nu)dE_\nu\right], \quad (12)$$

where σ_c is the cross section for the formation of the compound nucleus with He^3 ions, $\sigma_\nu(E_\nu)$ is the capture cross section of the emitted particle ν, and the remaining symbols are defined in Sec. VI 2.

We can obtain values of the cross sections for the formation of the compound nuclei σ_c with an optical-model calculation based on the Woods-Saxon potential.[41] No elastic-scattering data exist for 10-MeV He^3 particles; our optical-model reaction cross sections are based on parameters deduced from 12-MeV He^3 elastic scattering on Fe^{54}.[42] If the Woods-Saxon potentials are given by

$$V(r)=V_0/\{1+\exp[(r-r_0A^{1/3})/a]\}$$

and

$$W(r)=W_0/\{1+\exp[(r-r_aA^{1/3})/b]\}, \quad (13)$$

then $V_0=96.4$ MeV, $r_0=1.07$ F, $a=0.854$ F, $W_0=10$ MeV, $r_a=1.81$ F, and $b=0.592$ F. We assume a square charge distribution with $r_c=1.4A^{1/3}$ F. The calculated 10-MeV He^3 cross sections are $\sigma_c=368$ mb for Fe^{56} and $\sigma_c=252$ mb for Cu^{63}.[43]

In calculating the differential cross sections, we use the experimentally determined nuclear level parameters a, discussed in Sec. VI. The experimental $Fe^{56}(He^3,p)$ and $Cu^{63}(He^3,p)$ energy spectra and the corresponding

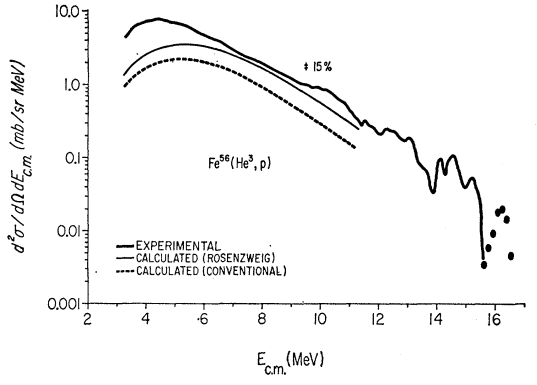

FIG. 15. Comparison of experimental $Fe^{56}(He^3,p)$ proton spectrum with statistical theory absolute values of the $Fe^{56}(He^3,p)Co^{58}$ spectrum. The two calculations are based on nuclear level densities with and without Rosenzweig energy shift.

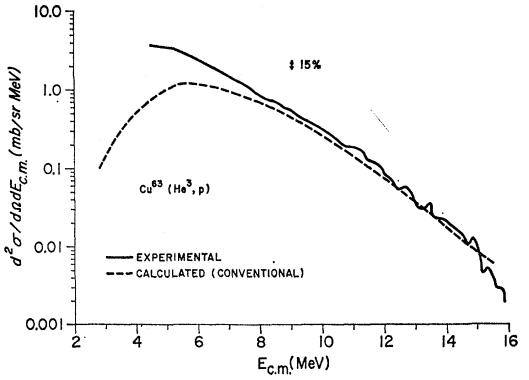

FIG. 16. Comparison of experimental $Cu^{63}(He^3,p)$ proton spectrum with statistical theory absolute values of the $Cu^{63}(He^3,p)Zn^{65}$ spectrum.

cross sections calculated with Eqs. (5) and (12) are shown in Figs. 15 and 16, respectively. These calculations only apply to the spectra resulting from the emission of protons from the primary compound nucleus; multiple particle emissions are not included. In Sec. VII 3 we present calculations which indicate that the proton spectra corresponding to proton kinetic energies greater than 6 MeV consist almost entirely of protons emitted from the primary compound nucleus. If we compare only the portions of the calculated and experimental energy spectra corresponding to protons emitted from the primary compound nucleus, the experimental and calculated $Cu^{63}(He^3,p)$ curves are found to differ by only 10%. The same comparison of the calculated and experimental $Fe^{56}(He^3,p)$ spectra yields a difference of 100%.

2. Calculation Including Shell Effects

We can include the effect of nuclear shell structure in the calculation of the $Fe^{56}(He^3,p)Co^{58}$ cross sections by replacing the nuclear level density expression $\rho(U_\nu-\Delta U_\nu)$ given by Eq. (5) with an expression similar to that obtained by Rosenzweig, Eq. (6):

$$\rho(U_\nu+\Delta U_\nu)=(\text{const})(U_\nu+\Delta E-\Delta U_\nu)^{-2}$$
$$\times\exp\{2[a(U_\nu+\Delta E-\Delta U_\nu)]^{1/2}\}, \quad (14)$$

where the Rosenzweig energy shift ΔE and the pairing energy ΔU_ν are defined in Sec. IV.[44,45] A different value of ΔE must be calculated with Eq. (7) for each of the different residual nuclei corresponding to the $Fe^{56}(He^3,n)$, $Fe^{56}(He^3,p)$, and $Fe^{56}(He^3,\alpha)$ reactions. As can be seen in Fig. 15 the agreement between the

[41] R. D. Woods and D. S. Saxon, Phys. Rev. **95**, 577 (1954).

[42] We are indebted to Dr. G. R. Satchler for communicating the values of the optical-model parameters for He^3.

[43] We are indebted to Dr. R. H. Bassel for a second, independent calculation of σ_c for 10-MeV He^3 particles incident upon Fe^{56}. Using the Oak Ridge Program plus optical-model parameters deduced from 12-MeV He^3 elastic scattering on Fe^{54} and on neighboring elements, Bassel obtained $\sigma_c=360$ mb.

[44] We have not derived Eq. (14) from first principles. Whether or not the term preceding the exponential term is to the -2 power as in Eq. (14) or to the $-\frac{5}{4}$ power as in Eq. (6) does not significantly change the value of the parameter a that is deduced from the experimental $Fe^{56}(He^3,p)$ cross sections.

[45] The similarity in the definitions of δ Eqs. (1) and (2) and Δ Eq. (6) indicate that these two parameters should be approximately equal. We therefore use the nuclear level density parameter a in Eq. (14).

statistical theory calculations and the experimental cross sections is significantly improved when Eq. (14) is used for the nuclear level density expression.

As a check for consistency, we have redetermined the value of the nuclear parameter a from the $Fe^{56}(He^3,p)Co^{58}$ data with a semilogarithmic plot based on Eq. (14). The slope of a semilogarithmic plot of

$$(d^2\sigma/d\Omega dE_\nu)(U_\nu-\Delta U_\nu+\Delta E)^2/E_\nu\sigma_\nu(E_\nu)$$

as a function of $(U_\nu-\Delta U_\nu+\Delta E)^{1/2}$ yields $a=8.7$ MeV^{-1}, the same value of a as determined in Fig. 11 with expression (10). The introduction of the Rosenzweig energy shift ΔE does not result in a change in the parameter a, but does significantly change the magnitude of the cross sections calculated with Eq. (12).[46]

An alternate approach to the inclusion of nuclear shell effects in the calculation of the $Fe^{56}(He^3,p)Co^{58}$ spectrum is not to use the Rosenzweig energy shift ΔE, but to use a different value of the nuclear level density parameter a in Eq. (5) for each of the different species of residual nuclei produced by the (He^3,n), (He^3,p), and (He^3,α) reactions.[3,4,20] If we use an expression such as the Newton-Lang recipe for a, Eq. (3), we find that the divergence between the magnitudes of the experimental $Fe^{56}(He^3,p)$ cross sections and the theoretical cross sections actually becomes greater than when the parameter a is kept constant ($a=8.7$ MeV^{-1}).[47]

The relative success of the Rosenzweig nuclear level density equation may be due to the fact that the effects of nucleon rearrangements in partially filled nuclear shells are included. According to the extreme shell model (no residual interactions) an unfilled shell with n nucleons and degeneracy g has a nuclear level density equal to $g!/[(g-n)!\,n!]$ at zero excitation energy.[2] Rosenzweig used a very simple model in order to obtain a closed-form expression, but his model, used to derive Eq. (6), does allow such rearrangements. Bloch has pointed out that changing the value of the parameter a according to Eq. (3) does not take the effect of nucleon rearrangements into consideration.[2,7,8,48]

3. Calculation of Cascade Emission Cross Sections

In preceding sections we considered only the emission of neutrons, protons, and alpha particles from the original compound nucleus; a divergence between the calculated single-particle emission cross sections and the experimental cross sections would therefore be expected in the regions of the spectra corresponding to low proton kinetic energies. The contributions of cascade emissions, i.e., the (He^3,np) and $(He^3,2p)$ reactions, can be included in the statistical theory calculations. The statistical theory calculation of cascade emission cross sections has been described by Blatt and Weisskopf.[36,49,50]

In our He^3+Cu^{63} cascade particle emission cross section calculation we employ the nuclear level density expression given by Eq. (5); whereas, in our He^3+Fe^{56} cascade particle emission cross section calculation we employ the nuclear level density expression with the Rosenzweig energy shift ΔE given by Eq. (14). Equation (7) was used to calculate the value of ΔE for each species of residual nucleus. Both the Fe^{56} and Cu^{63} calculations include competition between neutron, proton, and alpha particle emission. The value of a used for the residual nuclei resulting from the $Fe^{56}(He^3,p)$, $Fe^{56}(He^3,n)$, $Fe^{56}(He^3,\alpha)$, $Fe^{56}(He^3,np)$, and $Fe^{56}(He^3,2p)$ reactions is 8.7 MeV^{-1}. The value of a in the corresponding Cu^{63} reactions is 7.0 MeV^{-1}. The contribution from the $(He^3,\alpha p)$ reactions was insignificant.

If we assume that gamma emission takes precedence over the emission of protons with a kinetic energy of 2 MeV or less, we obtain the cross sections shown in Figs. 17 and 18.[51] The inclusion of the (He^3,np) and $(He^3,2p)$ reactions improves the agreement between the experimental and calculated curves.

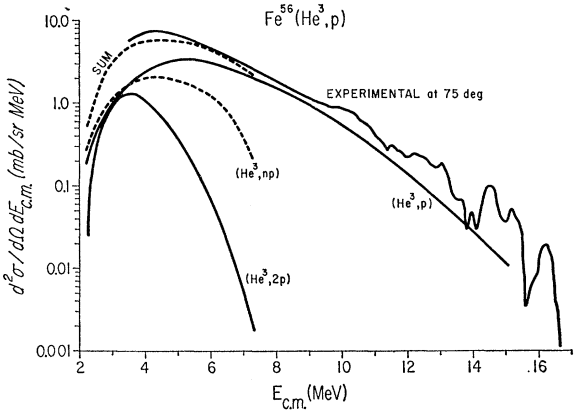

FIG. 17. Comparison of the experimental $Fe^{56}(He^3,p)$ spectrum with the sum of the statistical theory calculations of the $Fe^{56}(He^3,p)Co^{58}$, $Fe^{56}(He^3,np)Co^{57}$, and $Fe^{56}(He^3,2p)Fe^{57}$ spectra. The Rosenzweig level density equation was used in the statistical theory calculations.

[46] If we assume that $\delta=\Delta$, then $a=(\pi^2/6)\Delta^{-1}=(g/\gamma+e/\epsilon)$. The values of g, γ, e, and ϵ discussed in Sec. IV can then be used to obtain $a=6.6$ MeV^{-1}. The very simplified nuclear model employed by Rosenzweig should be considered when the value of 6.6 MeV^{-1} is compared to the empirical value 8.7 MeV^{-1}.

[47] If we employ Eq. (13) to calculate the value of a for Co^{58}, we obtain $a=6.7$ MeV^{-1}.

[48] Bloch, Ref. 2, explicitly considers the nucleon rearrangements of the extreme shell model without resorting to the simple model used by Rosenzweig. Unfortunately, Bloch's result for the nuclear level density is unwieldy and not in a neat closed form. At high excitation energies Bloch's nuclear level density expression approaches the level density expression used by Newton.

[49] We are indebted to Dr. H. M. Blann for kindly offering the use of his FORTRAN program for multiple-particle-emission cross sections.

[50] We would like to thank Mrs. N. S. Merkel for her desk computer calculation of the (He^3,np) and $(He^3,2p)$ statistical theory cross sections.

[51] This assumption about the competition between proton and gamma-ray emission is somewhat arbitrary. Nevertheless, an explicit assumption about competition between proton and gamma de-excitation is necessary in multiple-particle-emission cross-section calculations of the type described in Ref. 36.

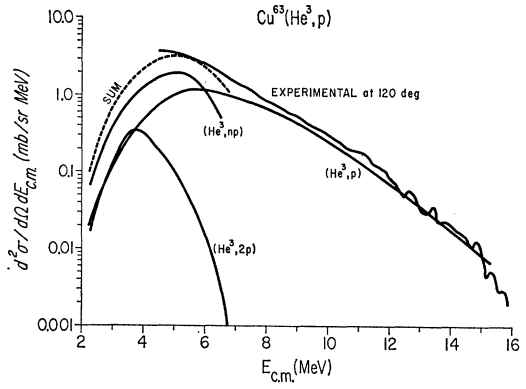

FIG. 18. Comparison of the experimental $Cu^{63}(He^3,p)$ spectrum with the sum of the statistical theory calculations of the $Cu^{63}(He^3,p)Zn^{65}$, $Cu^{63}(He^3,np)Zn^{64}$, and $Cu^{63}(He^3,2p)Cu^{64}$ spectra. The Rosenzweig level density equation was not used.

The complications in the interpretation of the experimental cross sections which occur because of the emission of particles in cascade could have been avoided by reducing the He^3 bombarding energy to a value at which cascade emissions are impossible. This approach, however, would create other problems. The Fe^{56} and Cu^{63} capture cross sections are steeply decreasing functions of He^3 energy, but the contaminating $O^{16}(He^3,p)$ and $C^{12}(He^3,p)$ cross sections are not. A reduction in bombarding energy would, therefore, be accompanied by a relative increase in $O^{16}(He^3,p)$ and $C^{12}(He^3,p)$ contamination. The decrease in Fe^{56} and Cu^{63} capture cross sections that would have resulted from a reduction in beam energy would have also required very long counting times. The He^3 beam current available at the Rochester 27-in. cyclotron was only 0.01 to 0.03 μA.

VIII. SUMMARY AND CONCLUSIONS

Large segments of the measured $Fe^{56}(He^3,p)$ and $Cu^{63}(He^3,p)$ energy and angular distributions are consistent with the statistical theory of nuclear reactions. The values of the nuclear level density parameter a deduced from the proton spectra are generally consistent with the values obtained by other authors.

Competition between the (He^3,n) and (He^3,p) reactions plays a significant role in the statistical theory calculation of (He^3,p) cross sections. The production of the Co^{58} residual nucleus by the $Fe^{56}(He^3,p)Co^{58}$ reaction competes with the production of the closed shell Ni^{58} residual nucleus by the $Fe^{56}(He^3,n)Ni^{58}$ reaction. Two different statistical theory calculations were compared with the experimental $Fe^{56}(He^3,p)$ cross-section measurements. The first calculation, the results of which are shown in Fig. 15, was based on Eq. (5) and did not consider the influence of nuclear shell effects on nuclear level densities. In this calculation the statistical theory cross section differs from the experimental cross section by a factor of 2. In a second calculation, the results of which are also shown in Fig. 15, the effect of nuclear shell structure on nuclear level densities was taken into consideration by using a nuclear level density expression derived by Rosenzweig. The agreement between experimental and calculated absolute $Fe^{56}(He^3,p)$ cross sections was significantly improved.

The residual nuclei involved in the competing (He^3,n) and (He^3,p) decay modes of the Ga^{66} compound nucleus, produced by the He^3+Cu^{63} reaction, are relatively far removed from the 28 nucleon closed shells. Consequently, the very degenerate discrete nucleon level model used by Rosenzweig would not be applicable. A conventional statistical theory calculation based on Eq. (5) yields absolute cross sections which substantially agree with the experimental $Cu^{63}(He^3,p)$ cross sections, Fig. 16.

A final set of statistical theory calculations which include contributions of cascade emissions by the (He^3,np) and $(He^3,2p)$ reactions are compared with the Fe^{56} and Cu^{63} experimental cross sections in Figs. 17 and 18.

A similar, but more clear-cut, experimental investigation of the influence of nuclear shell structure on nuclear level densities at relatively high excitation energies than is illustrated by the competition between the $Fe^{56}(He^3,p)Co^{58}$ and $Fe^{56}(He^3,n)Ni^{58}$ reactions could probably be based on a comparison of the competition between the $Fe^{54}(He^3,p)Co^{56}$ and the $Fe^{54}(He^3,n)Ni^{56}$ reactions. Nuclear shell effects should greatly influence the competition between the production of Co^{56} and the doubly closed shell Ni^{56} residual nuclei.[2-6]

ACKNOWLEDGMENTS

The authors would like to acknowledge the help and suggestions of Dr. H. M. Blann; we would also like to express our gratitude for the kind offer of his multiple particle emission FORTRAN program. One of us (J. P. H.) would also like to thank Dr. Blann for his guidance and encouragement during his graduate work. We wish to express our appreciation to Dr. W. P. Alford and Dr. D. Cline for the loan of their multiplier and their excellent aid and encouragement. The courtesy and assistance of Dr. E. O. Wiig are gratefully acknowledged. One of the authors (J. P. H.) wishes to thank Dr. H. W. Fulbright for his valuable suggestions and encouragement. The authors would also like to thank Dr. L. Blau and Dr. R. West for their advice and assistance. We are indebted to G. Hartquist for his efficient operation of the 27-in. cyclotron. Recognition is extended to Dr. A. Ewart for stimulating discussions. One of the authors (J. P. H.) wishes to thank the United States Education Committee in France, whose Fulbright travel grant enabled him to study abroad.